A&A 608, A84 (2017)
DOI: 10.1051/0004-6361/201731382

Astronomy & Astrophysics

Solving the conundrum of intervening strong Mg II absorbers towards gamma-ray bursts and quasars⋆

L. Christensen[1], S. D. Vergani[2,3], S. Schulze[4], N. Annau[5,1], J. Selsing[1], J. P. U. Fynbo[1], A. de Ugarte Postigo[6,1], R. Cañameras[1], S. Lopez[7], D. Passi[7], P. Cortés-Zuleta[7], S. L. Ellison[5], V. D'Odorico[8], G. Becker[9], T. A. M. Berg[5], Z. Cano[6], S. Covino[10], G. Cupani[8], V. D'Elia[11,12], P. Goldoni[13], A. Gomboc[14], F. Hammer[2], K. E. Heintz[15,1], P. Jakobsson[15], J. Japelj[16], L. Kaper[16], D. Malesani[1], P. Møller[17], P. Petitjean[3], V. Pugliese[16], R. Sánchez-Ramírez[6,18], N. R. Tanvir[19], C. C. Thöne[6], M. Vestergaard[1,21], K. Wiersema[19], and G. Worseck[20]

[1] Dark Cosmology Centre, Niels Bohr Institute, University of Copenhagen, Juliane Maries Vej 30, 2100 Copenhagen, Denmark
e-mail: lise@dark-cosmology.dk
[2] GEPI, Observatoire de Paris, PSL Research University, CNRS, place Jules Janssen, 92190 Meudon, France
[3] Institut d'Astrophysique de Paris, Université Paris 6-CNRS, UMR7095, 98bis boulevard Arago, 75014 Paris, France
[4] Department of Particle Physics and Astrophysics, Weizmann Institute of Science, 7610001 Rehovot, Israel
[5] Department of Physics and Astronomy, University of Victoria, Victoria, BC V8P 1A1, Canada
[6] Instituto de Astrofísica de Andalucía (IAA-CSIC), Glorieta de la Astronomía s/n, 18008 Granada, Spain
[7] Departamento de Astronomía, Universidad de Chile, Casilla 36-D, 1058 Santiago, Italy
[8] INAF–Osservatorio Astronomico di Trieste, via Tiepolo 11, 34143 Trieste, Italy
[9] Department of Physics and Astronomy, University of California, Riverside, CA 92521, USA
[10] INAF–Osservatorio Astronomico di Brera, via Bianchi 46, 23807 Merate (LC), Italy
[11] INAF–Osservatorio Astronomico di Roma, via Frascati 33, 00040 Monteporzio Catone, Italy
[12] ASI-Science Data Centre, via del Politecnico snc, 00133 Rome, Italy
[13] APC, Univ. Paris Diderot, CNRS/IN2P3, CEA/Irfu, Obs. de Paris, Sorbonne Paris Cité, 75013 Paris, France
[14] Centre for Astrophysics and Cosmology, University of Nova Gorica, Vipavska 11c, 5270 Ajdovščina, Slovenia
[15] Centre for Astrophysics and Cosmology, Science Institute, University of Iceland, Dunhagi 5, 107 Reykjavík, Iceland
[16] Anton Pannekoek Institute for Astronomy, University of Amsterdam, Science Park 904, 1098 XH Amsterdam, The Netherlands
[17] European Southern Observatory, Karl-Schwarzschild-Strasse 2, 85748 Garching bei München, Germany
[18] INAF, Istituto di Astrofisica e Planetologia Spaziali, Via Fosso del Cavaliere 100, 00133 Roma, Italy
[19] Department of Physics and Astronomy, University of Leicester, Leicester LE1 7RH, UK
[20] Max-Planck-Institut für Astronomie, Königstuhl 17, 69117 Heidelberg, Germany
[21] Dept. of Astronomy, Steward Observatory, University of Arizona, 933 North Cherry Avenue, Tucson, AZ 85721, USA

Received 15 June 2017 / Accepted 1 September 2017

ABSTRACT

Previous studies have shown that the incidence rate of intervening strong Mg II absorbers towards gamma-ray bursts (GRBs) were a factor of 2–4 higher than towards quasars. Exploring the similar sized and uniformly selected legacy data sets XQ-100 and XSGRB, each consisting of 100 quasar and 81 GRB afterglow spectra obtained with a single instrument (VLT/X-shooter), we demonstrate that there is no disagreement in the number density of strong Mg II absorbers with rest-frame equivalent widths $W_r^{\lambda 2796} > 1$ Å towards GRBs and quasars in the redshift range $0.1 \lesssim z \lesssim 5$. With large and similar sample sizes, and path length coverages of $\Delta z = 57.8$ and 254.4 for GRBs and quasars, respectively, the incidences of intervening absorbers are consistent within 1σ uncertainty levels at all redshifts. For absorbers at $z < 2.3$, the incidence towards GRBs is a factor of 1.5 ± 0.4 higher than the expected number of strong Mg II absorbers in Sloan Digital Sky Survey (SDSS) quasar spectra, while for quasar absorbers observed with X-shooter we find an excess factor of 1.4 ± 0.2 relative to SDSS quasars. Conversely, the incidence rates agree at all redshifts with reported high-spectral-resolution quasar data, and no excess is found. The only remaining discrepancy in incidences is between SDSS Mg II catalogues and high-spectral-resolution studies. The rest-frame equivalent-width distribution also agrees to within 1σ uncertainty levels between the GRB and quasar samples. Intervening strong Mg II absorbers towards GRBs are therefore neither unusually frequent, nor unusually strong.

Key words. quasars: absorption lines – gamma rays: general – galaxies: halos

1. Introduction

Luminous point sources, gamma-ray bursts (GRBs) and quasars, are efficient probes of the gaseous material along their lines of sight. Both classes of objects are currently detected out to $z > 7$ (Tanvir et al. 2009; Salvaterra et al. 2009; Mortlock et al. 2011) and thus probe a very long path length through the universe.

⋆ Based on observations collected at the European Southern Observatory, Paranal, Chile, Program ID: 098.A-0055, 097.A-0036, 096.A-0079, 095.B-0811(B), 095.A-0045, 094.A-0134, 093.A-0069, 092.A-0124, 0091.C-0934, 090.A-0088, 089.A-0067, 088.A-0051, 087.A-0055, 086.A-0073, 085.A-0009 and 084.A-0260. XQ-100: 189.A-0424.

Table 1. Strong Mg II absorber searches in the literature.

Reference	N_{obj}	$N_{Mg\,II}$	Δz	$\langle z \rangle$	Excess/SDSS	Excess/high-res
Low-redshift absorbers ($z_{Mg\,II} < 2.3$)						
Prochter et al. (2006b)	14	14	15.5	1.1	≈3.8	
Sudilovsky et al. (2007)	5	6	6.75	1.3	≈4	
Tejos et al. (2009)	8	9	10.86	1.34	$3.0^{+1.5}_{-1.1}$	
Bergeron et al. (2011; blazars)	45	13	29.93	0.82	$2.2^{+0.8}_{-0.6}$	
Vergani et al. (2009; high res.)	10	9	13.94	1.11	≈2	
Vergani et al. (2009; high+low res.)	26	22	31.55	1.3	2.1 ± 0.6	
Cucchiara et al. (2013; high res.)	18	13	20.3	1.1	2.6 ± 0.8	
Cucchiara et al. (2013; high+low res.)	95	20	55.5	1.15	1.5 ± 0.4	
This work (GRBs from XSGRB)	81	18	44.71	1.22	1.48 ± 0.35	1.11 ± 0.28
This work (quasars)	100	52	110.5	1.74	1.37 ± 0.19	1.02 ± 0.18
High redshift absorbers ($z_{Mg\,II} > 2.3$)						
This work (GRBs from XSGRB)	81	5	13.14	3.28		0.71 ± 0.34
This work (quasars)	100	45	143.9	3.04		0.56 ± 0.93

Notes. N_{obj} lists the GRB or quasar sample sizes, and $N_{Mg\,II}$ is the number of detected absorbers within the total redshift path length, Δz, with an average redshift, $\langle z \rangle$. The penultimate column lists the reported excess of absorbers relative to the expectation from SDSS quasar absorber statistics. One exception is that Bergeron et al. (2011) analysed blazars rather than GRBs. Vergani et al. (2009) and Cucchiara et al. (2013) reported statistics from high-spectral-resolution data, as well as combined high- and low-spectral-resolution data. It should be noted that there are substantial overlaps of the target selections amongst the references, and the reported overdensities are therefore correlated. To compare our searches with the literature, we report statistics from absorbers at different redshift ranges: $z < 2.3$ and $z > 2.3$ (Sect. 3.2). The last column reports overdensities relative to high-spectral-resolution quasar studies by Mathes et al. (2017) for the low-redshift sample, and Chen et al. (2016) for the high-redshift sample.

Absorption lines at various redshifts in the spectra of the background sources provide us with methods to explore the high-redshift universe in absorption even though the galaxies that cause the absorption lines are not detected in emission. Since both GRBs and quasars probe intervening material randomly, it was a puzzling discovery a decade ago that GRBs apparently had four times as many strong intervening Mg II absorbers with rest-frame equivalent widths $W_r^{\lambda 2796} > 1$ Å as did quasars (Prochter et al. 2006b). The same conclusion about Mg II absorber statistics was reached by Sudilovsky et al. (2007), with the addition that the incidence rate of C IV absorbers and weak Mg II absorbers with $W_r < 1$ Å did agree between the two background source types (Tejos et al. 2007, 2009; Vergani et al. 2009). Also, blazars were found to have twice as many strong Mg II absorbers as did quasars (Bergeron et al. 2011). Exploring high-spectral-resolution VLT/UVES data of GRB afterglows with high signal-to-noise ratios (S/N), Vergani et al. (2009) and Tejos et al. (2009) found an excess towards GRBs a factor of 2–3 higher than towards Sloan Digital Sky Survey (SDSS) quasars, and with only a 2σ confidence level of the over-abundance. Table 1 presents a summary of previous searches and reported excesses of strong Mg II systems. As the discrepancy between the absorber statistics has only been reported for strong Mg II absorbers with $W_r^{\lambda 2796} > 1$ Å, in this work we focus exclusively on these strong systems, unless specifically stated otherwise.

The excess number of absorbers has been suggested to be caused by either dust biases, partial covering and differences in source sizes, gravitational magnification, or the influences from the immediate environments of the GRBs, or intrinsic to the sources (Prochter et al. 2006b; Porciani et al. 2007; Frank et al. 2007; Ménard et al. 2008; Cucchiara et al. 2009; Vergani et al. 2009; Budzynski & Hewett 2011; Rapoport et al. 2013). Any effect of a partial coverage and source sizes was excluded based on statistics of absorbers towards the quasar broad line regions (Pontzen et al. 2007; Lawther et al. 2012). Some studies were hampered by relatively small GRB afterglow sample sizes and non-uniform data sets. Cucchiara et al. (2013) compiled a large data set collected from various telescopes and with a range of spectral resolutions, and demonstrated that the low- to intermediate-resolution data showed consistent values of strong Mg II absorbers between GRBs and quasars. However, when including the original high-resolution data from Prochter et al. (2006b) the discrepancy remained.

Incidences (dN/dz, or sometimes referred to as $l(z)$) of Mg II systems in GRB spectra are commonly compared to strong Mg II absorbers in SDSS quasar spectra, where absorber identifications are performed by automated routines (Nestor et al. 2005; Prochter et al. 2006a; Zhu & Ménard 2013). In SDSS data release DR12, the number of SDSS quasar spectra (~300 000 in Pâris et al. 2017) vastly outnumber GRB afterglow spectra (~300[1]) (Fynbo et al. 2009; de Ugarte Postigo et al. 2012), and so do the number of intervening Mg II absorbers (~37 000 in Raghunathan et al. 2016).

In this paper we revisit the Mg II puzzle by exploring newly collected homogeneous data sets obtained with a single instrument, X-shooter/VLT (Vernet et al. 2011). Data of 100 quasars were taken from the Legacy Large Programme, XQ-100 (Lopez et al. 2016), and 116 GRB spectra from the X-Shooter GRB legacy sample (XSGRB; Selsing et al., in prep., PI: Fynbo). These legacy data sets allow us to explore two unbiased and equally large sample sizes all obtained with a uniform spectral resolution and instrument setup. With these data, we expand the comparison of the Mg II absorber incidence to a larger redshift interval $0.14 < z < 5$. Section 2 describes the two data sets (GRB afterglows and quasars) and the search for strong absorbers. In Sect. 3 we derive incidence rates and equivalent width distributions, and compare with other studies in the literature. We then summarise in Sect. 4.

[1] `grbspec.iaa.es` presents afterglow spectra for 225 GRBs compiled until June, 2017 (de Ugarte Postigo et al. 2014).

2. Data sets and Mg II absorber detection

2.1. X-shooter spectral samples

The GRB afterglow spectra were collected in multiple semesters between 2009 and 2016 taking advantage of the X-shooter guaranteed program and subsequent open time proposals. With a uniform set of selection criteria for target-of-opportunity follow-up adopting the criteria for the low-resolution study of Fynbo et al. (2009), that is, mainly avoiding regions with high Galactic extinction and bursts near to the Sun, the total number of obtained afterglow spectra is 116 until October, 2016. All spectra were obtained with VLT/X-shooter, which provides intermediate spectral resolutions of $R = FWHM/\lambda \approx 6500-12\,000$ measured from UV to near-IR wavelengths. The S/N of the spectra vary as some afterglow spectra were obtained several hours to a few days after the GRB trigger, when only host spectral signatures and no characteristic power-law afterglow signature was visible. Removing these from the sample leaves 81 afterglow spectra, again with varying S/N between 1 and 50 per pixel for different bursts and wavelength coverage (see Selsing et al., in prep., for details). The data were reduced with the ESO VLT/X-shooter pipeline (Modigliani et al. 2010) managed by Reflex (Freudling et al. 2013), and with our own post-processing steps to improve the flux calibration and rejection of bad pixels (Selsing et al., in prep.) with reduction scripts made available online[2]. The redshifts of the GRBs lie in the range $0.256 < z < 6.32$.

Turning to the quasar sample, the XQ-100 survey is a VLT/X-shooter ESO Large Programme that targeted 100 quasars at $3.5 < z < 4.9$ with a S/N higher than 20 per pixel over the entire wavelength range (see Lopez et al. 2016, for details). The quasars were selected without prior knowledge of the presence of strong absorbers along our line of sight. The quasars and a large majority of GRB afterglows were observed with X-shooter slit widths of 1.0, 0.9, and 0.9 arcsec for the UVB, VIS, and NIR-arms, respectively, resulting in similar spectral resolutions between the two samples.

The redshift distributions of the GRB and quasar samples are shown in Fig. 1. By construction the quasars have a quite distinct distribution as high-redshift objects were selected, whereas there are no intrinsic constraints for the GRB redshift selection. To match the redshift distribution of GRBs we could include other quasars observed with X-shooter, using archive data. However, these quasars might have been selected on the basis of the presence or lack of any kind of intervening and intrinsic absorption line systems, so we do not expand the quasar sample beyond the XQ-100 data.

2.2. Additional data sets

Since the earlier discrepancy on the incidence of Mg II absorbers relied on the statistics of GRB absorbers obtained to that date, we also examined another large spectroscopic sample consisting of 60 low-resolution GRB afterglow spectra with known redshifts observed from 2005 to 2008. Intervening absorbers and their observed equivalent widths were compiled by Fynbo et al. (2009). These low-resolution spectra are also included in the Mg II statistics analysis by Cucchiara et al. (2013). In this work, the low-resolution data set is used as a comparison sample to the XSGRB data.

[2] https://github.com/jselsing/XSGRB_reduction_scripts

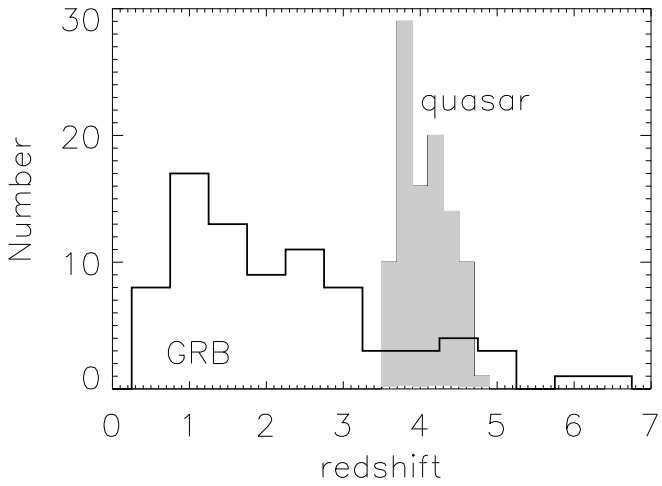

Fig. 1. Redshift distributions for the two background source samples (XQ-100 and XSGRB). The 81 GRB afterglows and 100 quasars have median redshifts of $z = 1.69$ and $z = 3.97$, respectively.

2.3. Redshift path length

The starting point of computing the strong Mg II absorber incidences is to determine the redshift path length (e.g. Lanzetta et al. 1987). Rather than relying on the sample sizes alone, the most relevant parameter for a survey is the total redshift path length where an absorber can be found.

X-shooter observes wavelengths down to 3000 Å, but because of a much reduced transmission below 3200 Å, we chose this latter wavelength to represent the lowest redshift for the detection of Mg II absorbers ($z = 0.14$).

For each object we created a top-hat function which was set to one between the redshifted Lyman-α line of the GRB/quasar and the wavelength of Mg II at the GRB/quasar redshift. The lower redshift limit excluded absorbers found in the Lyα forest because they are likely contaminated by intervening Lyα forest lines. We also excluded the region around 3000 km s^{-1} from the GRB/quasar redshifts, because absorbers detected in this region may be associated with the luminous background sources. These proximate absorbers have higher metallicities (Ellison et al. 2011) and different incidences (Ellison et al. 2002) showing that they do not probe a random intervening population. Rejecting the nearby regions decreased the redshift path lengths by $\Delta z = 0.02$–0.07 for each individual line of sight. Furthermore, we considered it impossible to find strong intervening absorbers in regions heavily affected by strong telluric lines when the transmission was less than ~30%, such as present between the J- and H, and H- and K bands. In these inaccessible regions the function was set to zero. Other wavelength regions are also affected by telluric absorption lines, but these absorption lines have been corrected for (Lopez et al. 2016; Selsing et al., in prep.), and do not pose a problem for detecting strong Mg II absorbers because their lines are much broader than the widths of telluric molecular absorption lines.

We also imposed a criterion for the spectral S/N. For the GRB spectra, we set the function to zero in any region where the S/N was less than three per spectral pixel (see Cucchiara et al. 2013, for a similar approach). A threshold of $S/N = 3$ corresponds to a 3σ detection limit $W_{\rm r,lim}^{\lambda 2796} \approx \sqrt{n_{\rm pix}} \times 2796$ Å$/R \approx 1$ Å, where R is the spectral resolution and $n_{\rm pix}$ is the number of pixels spanned by the absorption line. Resolutions were determined to be $R \sim 12\,000$ and $R \sim 6500$ from measuring the

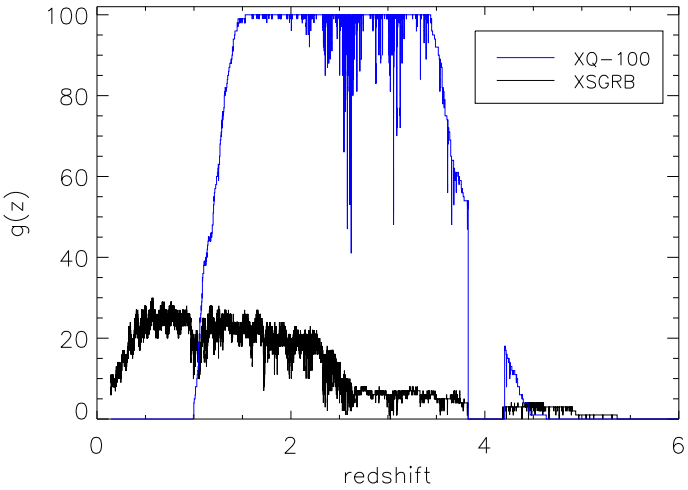

Fig. 2. Redshift path density for the two samples, with quasars shown in blue and GRB afterglows in black. The gap at $z \sim 4$ is caused by the atmospheric absorption bands between the J- and H bands, where no Mg II absorbers can be recognised. XQ-100 includes 100 sightlines, hence $g(z)$ saturates at this level.

FWHM of unresolved lines in the VIS and NIR arms, respectively (Selsing et al., in prep.).

We then added up these functions for all the GRB and quasar spectra, converted the observed wavelengths to the Mg II redshift values, and summed over all objects as a function of the absorber redshift. The resulting redshift path densities, $g(z)$, are presented in Fig. 2, and the integrated redshift path lengths $\Delta z = \int g(z)\mathrm{d}z$ are listed in Table 1.

2.4. Finding Mg II absorbers

As the discrepancy between Mg II absorber incidences refers to strong systems, we searched for absorbers with $W_\mathrm{r}^{\lambda 2796} > 1$ Å. Other species of atomic absorption lines, including lower equivalent width Mg II systems, will be presented elsewhere (for the XQ-100 sample in Lopez et al., in prep. and the GRB sample in de Ugarte Postigo et al., in prep.).

Strong Mg II lines with rest frame equivalent widths $W_\mathrm{r}^{\lambda 2796} > 1$ Å were independently visually identified by several of the authors. At the resolution of X-shooter, there is no problem in identifying strong Mg II $\lambda\lambda$2796, 2803 doublets visually as the lines are well separated. Additional confirmation of the doublet comes from identifying the transitions of Mg I λ2852 and Fe II λ2600 at the Mg II redshift, but this criterion did not exclude any candidate Mg II systems.

With the chosen criterion that the S/N level is >3 per pixel, visual identification of strong Mg II absorbers takes advantage of the doublet nature with lines for the strong absorbers always being broad and saturated. The higher S/N of the spectra in the XQ-100 sample meant that visual identification of strong Mg II absorbers was unambiguous, and the choice of S/N cut did not affect the final results. We verified that none of the identified strong absorbers fall in wavelength regions affected by any of the selection criteria. While the S/N per spectral pixel is modest for some spectra in the GRB sample, the absorption signature from the Mg II doublet plus additional absorption species covered many pixels (30–50), and therefore the integrated S/N of the absorption system is much larger than the simple pixel-by-pixel level of the signal. In total we identified 23 strong Mg II systems towards the 81 GRBs and 97 strong Mg II systems towards the 100 quasars. They are listed in Tables 2 and A.1, respectively. We computed the rest frame equivalent widths of the strongest line in the doublet, $W_\mathrm{r}^{\lambda 2796}$, by defining a continuum level region around the identified line with ~10 Å wide wavelength ranges bluewards and redwards of the Mg II doublet. Errors for W_r were computed by propagating the uncertainties from the associated error spectrum. In the case where two absorber components lie within 500 km s^{-1} from each other they were treated as a single system (similarly as in Chen et al. 2016), and W_r represents the sum of the components.

We excluded absorbers with $W_\mathrm{r}^{\lambda 2796} < 1$ Å even if their equivalent width, including uncertainties, could place them among the strong absorber sample. Since the quasar spectra have high S/N values, the uncertainties lie in the range $\Delta W_\mathrm{r} = 0.01-0.04$ Å. Although below the $W_\mathrm{r} > 1$ Å limit, including 1σ measurement uncertainties, five additional Mg II absorbers would pass for strong absorbers in the quasar sample and a single one in the GRB sample. These are also listed in Tables 2 and A.1 for completeness.

The transient nature of GRB afterglows prevents us from obtaining follow-up spectra at different wavelengths once the afterglow fades below detection limits. Therefore it is difficult to determine additional absorption properties of the strong intervening Mg II absorbers in the XSGRB sample, for example if the absorbers are metal-rich or strong depending on the hydrogen column densities. However, with alternative methods we

Table 2. Intervening strong Mg II absorbers in the GRB sample, with redshifts listed for the GRBs (z_GRB) and the absorbers (z_abs).

GRB name	z_GRB	z_abs	W_r^{2796} [Å]	D
GRB 090313A	3.373	1.801	1.86 ± 0.16	11.0 ± 0.9
GRB 100219A	4.667	1.856	1.02 ± 0.08	5.9 ± 0.5
		2.181	0.92 ± 0.19	10.5 ± 2.2
GRB 100316B	1.180	1.063	1.28 ± 0.08	6.2 ± 0.4
GRB 100901A	1.408	1.315	1.35 ± 0.28	2.1 ± 0.4[a]
GRB 111008A	4.990	4.610	4.25 ± 0.09	6.9 ± 0.1
GRB 111107A	2.893	1.998	2.60 ± 0.47	8.9 ± 1.6
GRB 120119A	1.728	1.214	1.65 ± 0.08	4.2 ± 0.2
GRB 120712A	4.175	2.102	2.99 ± 0.45	9.0 ± 1.4
GRB 120815A	2.359	1.539	6.26 ± 0.07	9.3 ± 0.1
GRB 121024A	2.300	1.959	1.24 ± 0.06	5.5 ± 0.3
GRB 121027A	1.773	1.459	1.91 ± 0.21	9.5 ± 1.0
GRB 121229A	2.707	1.659	1.33 ± 0.60	5.1 ± 2.3
GRB 130408A	3.758	3.016	2.96 ± 0.83	8.0 ± 2.3
GRB 130606A	5.913	3.451	1.65 ± 0.06	4.8 ± 0.2
GRB 131030A	1.294	1.164	1.95 ± 0.03	4.9 ± 0.1
GRB 140614A	4.233	2.113	1.39 ± 0.41	4.8 ± 1.4
GRB 141028A	2.332	1.820	3.23 ± 0.73	9.9 ± 2.2
GRB 141109A	2.993	2.504	2.00 ± 0.09	9.3 ± 0.4
		2.874	4.21 ± 0.25	10.1 ± 0.6
GRB 150403A	2.057	1.761	2.76 ± 0.05	9.9 ± 0.2
GRB 151021A	2.330	1.491	1.35 ± 0.33	7.1 ± 1.7
GRB 160203A	3.519	1.267	1.40 ± 0.19	4.0 ± 0.5
GRB 161023A	2.708	1.243	1.83 ± 0.02	7.1 ± 0.1

Notes. The list includes one absorber fulfilling the criterion that $W_\mathrm{r}^{2796} \gtrsim 1$ Å within its 1σ uncertainty. The D index refers to the definition by Ellison (2006). [(a)] This absorber has two distinct components separated by 390 km s^{-1} and the index refers to the sum of the components.

can address this issue for the Mg II absorbers. The damped Ly-α absorbers (DLAs) identified in XQ-100 (Sánchez-Ramírez et al. 2016; Berg et al. 2016) all show Mg II absorption lines (besides those that remain undetected in the gap between the J- and H bands), but only about half are classified as strong Mg II systems with $W_{\rm r}^{\lambda 2796} > 1$ Å (Berg et al. 2017). The D-index of Ellison (2006), defined as $D = (W_{\rm r}/\Delta V) \times 1000$, with ΔV being the full velocity width of the absorption line in km s^{-1} relative to the continuum, can be used as a criterion to pre-select DLA systems in cases where the hydrogen column density is unknown. The threshold value of the D-index for an absorber to be a DLA system depends on the observed spectral resolution. All DLAs found in the XQ-100 sample have $D > 4$ (Berg et al. 2017). In Table 2, we list the D-index for Mg II absorbers in the XSGRB sample, suggesting that all but one of the absorbers are DLAs.

In addition to the X-shooter samples, we examined the low-resolution GRB spectra by Fynbo et al. (2009) in the same manner as the X-shooter data. This sample was kept separate from the X-shooter GRB sample, and was used to look for any dependence on spectral resolution at lower redshifts. In the low-resolution sample we found 15 intervening strong Mg II systems at $0.2 < z < 2.2$ within a total path length of $\Delta z = 50.3$.

3. Statistics of strong Mg II systems

3.1. Incidence rate

Next we computed the incidence, or sometimes referred to as the line density:

$$\frac{{\rm d}N}{{\rm d}z} = \frac{\sum_{z_1}^{z_2} N_{\rm abs}}{\Delta z} = \frac{\sum_{z_1}^{z_2} N_{\rm abs}}{\int_{z_1}^{z_2} g(z){\rm d}z}, \quad (1)$$

in redshift intervals from z_1 to z_2. We experimented with several binning approaches in the analysis, as described below. Unless specified, in all experiments, the first bin starts at the minimum redshift in the path length, $z = 0.14$. We first chose bin sizes to include an equal number of absorbers in each bin, which gave irregular sizes of the redshift bins. For the quasar sample, we chose 20 Mg II systems in each bin, six for the XSGRB sample, and eight in the low-resolution GRB data. The numbers were chosen to have a similar number of bins for each sample in order to analyse the redshift evolution. With the small number of absorbers in the low-resolution data, however, there were only two bins.

To compute uncertainties of the incidences we assumed that the error is equal to $\sqrt{N_{\rm abs}}$ as given by Poisson statistics. However, because the square root approximation underestimates errors in the small number regime (Gehrels 1986), we also computed errors using a Monte Carlo bootstrapping with replacement technique. We created a random sample with replacements of 100 quasars (81 GRBs) and compute the path lengths, number of absorbers and incidences within the redshift intervals. The 1σ standard deviation of incidences from 1000 experiments, which represent the uncertainty, gave the same error as computed from the square root approximation for the Poisson statistics.

The results for the Mg II sample that passed the strict criterion that $W_{\rm r} > 1$ Å are illustrated in the left panel in Fig. 3 with computed incidences listed in Table 3. We find that the incidence of strong Mg II absorbers towards GRBs and quasars is consistent to within 1σ uncertainty levels at all redshifts.

Traditional methods for computing the incidence also work with a set of non-overlapping redshift bins. As a second method of binning, we computed the incidence of Mg II systems in the GRB and quasar samples using a sliding redshift bin technique (see Sánchez-Ramírez et al. 2016, for an application to compute the total neutral hydrogen density, $\Omega_{\rm DLA}$, with sliding bins). We chose redshift interval bin sizes of $\Delta z = 0.7$ and increased the steps above $z = 2.5$ to $\Delta z = 1.2$ for the GRB sample. The resulting 68% confidence intervals are shown in the grey and blue shaded regions in the left panel in Fig. 3. Choosing a larger Δz smooths out the curves, but the redshift evolution of the incidence rate does not change the overall shape. We also examined the result from using a sliding constant integrated path length, Δz (Sánchez-Ramírez et al. 2016). The two methods that we used for computing the incidence rates gave consistent results.

Table 3. Incidences for strong Mg II absorbers towards GRB and quasars at the median redshift interval $\langle z \rangle$.

GRB Mg II systems			
$\langle z \rangle$	$z_{\rm min} - z_{\rm max}$	${\rm d}N/{\rm d}z$	${\rm d}N/{\rm d}X$
0.802	0.144–1.459	0.215 ± 0.088	0.104 ± 0.043
1.639	1.459–1.818	0.788 ± 0.322	0.286 ± 0.117
2.161	1.818–2.503	0.511 ± 0.209	0.166 ± 0.068
3.557	2.503–4.610	0.547 ± 0.245	0.149 ± 0.067
Quasar Mg II systems			
$\langle z \rangle$	$z_{\rm min} - z_{\rm max}$	${\rm d}N/{\rm d}z$	${\rm d}N/{\rm d}X$
1.352	0.963–1.740	0.357 ± 0.087	0.149 ± 0.033
1.914	1.740–2.404	0.205 ± 0.109	0.166 ± 0.037
2.389	2.404–2.776	0.269 ± 0.084	0.116 ± 0.026
3.016	2.776–3.061	0.357 ± 0.063	0.079 ± 0.018
3.920	3.061–4.381	0.546 ± 0.111	0.119 ± 0.029

Notes. $z_{\rm min} - z_{\rm max}$ gives the redshift interval.

The incidence rates were also computed with the expanded samples that include absorbers with $W_{\rm r} > 1$ Å within $\sim 1\sigma$ measurement uncertainties. This addition does not change the results, and the agreement between incidences from the GRB and quasar samples remain consistent to within 1σ.

Another frequently used statistic related to absorbers is the comoving line density ${\rm d}N/{\rm d}X$ defined as

$$\frac{{\rm d}N}{{\rm d}X} = \frac{\sum_{z_1}^{z_2} N_{\rm abs}}{\Delta X}, \quad (2)$$

where the absorption distance is

$$\Delta X = \int_{z_1}^{z_2} g(z) \frac{(1+z)^2}{\sqrt{\Omega_{\rm m}(1+z)^3 + \Omega_\Lambda}} {\rm d}z. \quad (3)$$

We used $\Omega_{\rm m} = 0.308$ and $\Omega_\Lambda = 0.692$ from recent Planck analyses (Planck Collaboration XIII 2016). The results listed in Table 3 and shown in the right hand panel of Fig. 3 again demonstrate that the quasar and GRB incidence rates agree within 1σ uncertainty levels.

The comoving line density of quasar Mg II absorbers has been argued to evolve with redshift, with an increase from $z = 0$ to $z \sim 2$ (Nestor et al. 2005; Mathes et al. 2017) followed by a decrease towards higher redshifts (Matejek & Simcoe 2012; Chen et al. 2016). This trend roughly follows the redshift evolution of the comoving star formation rate density, suggesting that the strong absorbers somehow trace star formation activity (Ménard et al. 2011). In the analyses of GRB and quasar absorbers presented in this work, measurement uncertainties are

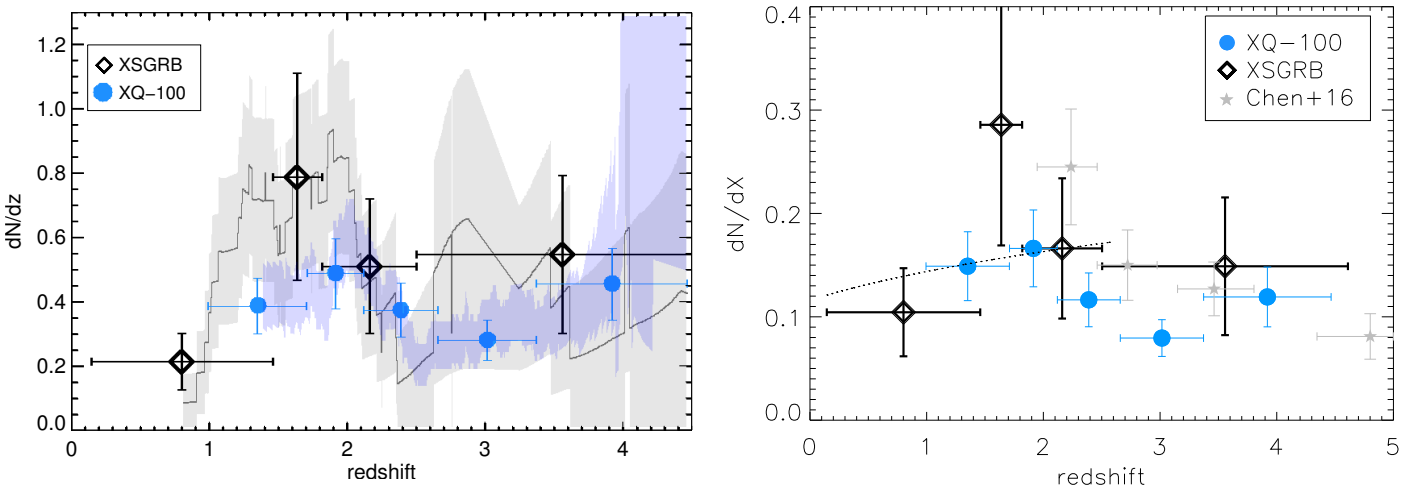

Fig. 3. *Left hand panel*: incidence rates from the two legacy samples of strong Mg II absorbers with points representing bin sizes with 6 and 20 absorbers in the XSGRB and XQ-100 samples, respectively. The grey line illustrates a sliding redshift binning of XSGRB absorbers and the shaded region presents the 68% confidence levels. The blue shaded region represents the 68% confidence intervals for a similar sliding redshift binning of the XQ-100 sample. *Right hand panel*: comoving line density. The dotted line represent strong Mg II absorbers in quasar spectra (Mathes et al. 2017), and the grey stars mark a larger sample of quasar absorbers at high redshifts (Chen et al. 2016).

large and do not probe the highest redshifts ($z > 5$). Nevertheless, number statistics agree with previous high-spectral-resolution studies (Matejek & Simcoe 2012; Chen et al. 2016).

3.2. Comparison between samples

Earlier analyses suggested that GRBs and quasars trace Mg II systems differently, and the excess incidence of strong Mg II absorbers are frequently computed relative to SDSS quasar spectra. In order to compare numbers with the overdensities listed in Table 1, we computed the expected number of strong absorbers by integrating

$$N_{\rm exp} = \int_{z_1}^{z_2} g(z) \frac{\partial N}{\partial z} {\rm d}z, \quad (4)$$

from $z_1 = 0.14$ to $z_2 = 2.3$, where the functional form for the SDSS Mg II incidence $\frac{\partial N}{\partial z}$ was taken from Zhu & Ménard (2013) and $g(z)$ from Fig. 2. The expected numbers of Mg II absorbers are 12.1 and 37.9 for the XSGRB and XQ-100 samples, respectively, while we found 18 and 52 absorbers. Both samples therefore suggest an excess factor of 1.48 ± 0.35 and 1.37 ± 0.19 relative to SDSS quasars, while the incidences in this redshift interval are consistent between our quasar and GRB samples within 0.3σ uncertainties.

Whereas the incidences from the two legacy samples are consistent with each other, we proceed to compare incidences to other samples of intervening strong Mg II absorbers towards GRB reported in the literature and to SDSS quasars. In Fig. 4 all GRB samples have black symbols and quasar samples are shown in blue. The large black diamonds that represent the XSGRB sample show that the incidence rate from GRBs at $0.144 < z < 1.449$ agrees with incidence rate from SDSS quasars illustrated by the dashed and dotted curves (Prochter et al. 2006a; Zhu & Ménard 2013), while the bin for GRBs at $1.459 < z < 1.818$ suggests a larger incidence of ${\rm d}N/{\rm d}z = 0.788 \pm 0.322$ (Table 3) which is an excess factor of 2.3 ± 0.9 compared to ${\rm d}N/{\rm d}z = 0.354 \pm 0.005$ expected from the SDSS (Zhu & Ménard 2013). To compute uncertainties for the SDSS incidence we fit ${\rm d}N/{\rm d}z$ (Fig. 13 in Zhu & Ménard 2013) with a 3rd-order polynomial function following the results by Prochter et al. (2006a) and calculated the covariance matrix from which we derived 68% confidence intervals.

In Fig. 4 the points at $z \sim 1$ from Prochter et al. (2006b) and at $z \sim 0.7$ from Vergani et al. (2009)[3] suggest incidences that have an excess of a factor of 3.8 and 2, although consistent to within 1.5–2σ uncertainties from the SDSS. Cucchiara et al. (2013) determined an average incidence ${\rm d}N/{\rm d}z = 0.18 \pm 0.06$ in a broad redshift range $0.36 < z < 2.2$ based on their own independently collected sample of 83 GRBs. Their full sample consisted of 95 high- and low-resolution afterglow spectra and included previously published data from the literature which gave a higher incidence of 0.36 ± 0.09. Compared to ${\rm d}N/{\rm d}z = 0.24$ expected from SDSS quasars, they derived an excess factor of 1.5 ± 0.4. In the same redshift interval for GRB absorbers we derived ${\rm d}N/{\rm d}z(z = 0.36$–$2.2) = 0.42 \pm 0.10$, that is, consistent within 0.5σ uncertainty incidences from the total sample in Cucchiara et al. (2013).

We examined if any Mg II absorbers were potentially missed in the SDSS samples by cross matching SDSS Mg II absorbers in the study by Raghunathan et al. (2016) with the XQ-100 sample. In total, 17 quasars are in common, and for these sight lines the detected strong absorbers mostly agree. One of the SDSS spectra suggests $W_{\rm r}$ below the 1 Å criterion, whereas in the XQ-100 data the criterion is fulfilled, and reversely for one other case. Only a single strong Mg II system at $z \sim 2$ was missed in the SDSS data (SDSS J105705+191041). The number of objects in common in XQ-100 and in Raghunathan et al. (2016) is insufficient to demonstrate if the SDSS is missing any absorbers since XQ-100 does not probe absorbers below $z = 1$. More detailed investigations including lower-redshift quasars are needed to determine if other absorbers could be missed in the SDSS.

3.3. Comparison with high-spectral-resolution quasar data

While the SDSS database of quasar spectra provides the largest sample for comparison in terms of number statistics, other large samples of quasar spectra have been compiled. Using archival high-spectral-resolution data from Keck/HIRES and

[3] Bergeron et al. (2011) present a correction to the numbers given by Vergani et al. (2009) and we use the corrected incidences here.

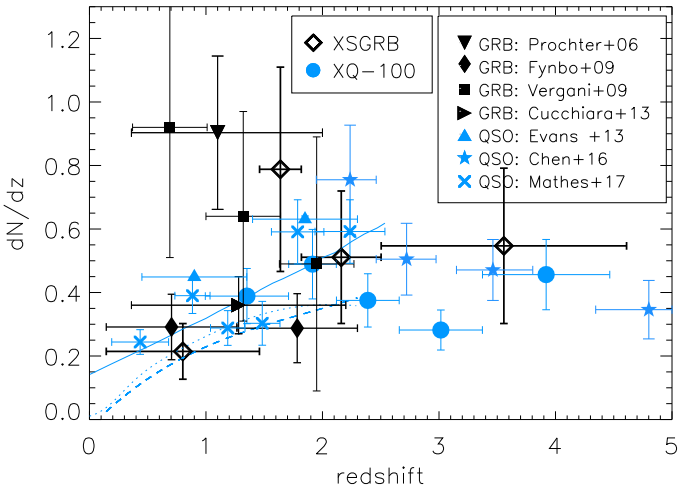

Fig. 4. Incidences from the literature for both GRB and quasar absorbers. Symbols are colour coded with all quasar samples shown in blue and GRB samples in black. Incidences from the low-spectral-resolution GRB sample from Fynbo et al. (2009) were re-analysed in this work. This low-resolution data set is also part of the sample compiled by Cucchiara et al. (2013). The dashed and dotted curves show expectations from SDSS quasar data from Prochter et al. (2006a) and Zhu & Ménard (2013), respectively, and the solid line the incidence towards quasars measured with high-spectral-resolution data (Mathes et al. 2017).

VLT/UVES, Evans et al. (2013) investigated Mg II systems in 252 quasar spectra, and determined an incidence of strong absorbers $dN/dz = 0.449 \pm 0.003$ at $z < 1.4$, consistent with our result within 1σ errors, but above the average SDSS incidence ($dN/dz(z = 0.43-1.4) = 0.256 \pm 0.003$) by a factor of 1.75 ± 0.02. They also found that more luminous quasars at $0.4 < z < 2.3$ have statistically significantly fewer absorbers than fainter quasars, but the difference in incidence rates is only a 20% effect. In a compiled sample of 602 high-resolution quasar spectra, again obtained from archival UVES and HIRES data, Mathes et al. (2017) analysed Mg II absorbers at $0.14 < z < 2.64$ (blue crosses in Fig. 4) and found increasing incidences at $z \sim 2$ compared to lower redshifts, generally consistent with the redshift evolution of absorbers seen in SDSS spectra, although the incidences found by Mathes et al. (2017) are 2σ higher at redshift bins $z < 1.1$ and $z > 1.5$.

While we computed an excess of strong Mg II absorbers relative to the SDSS quasars, the incidences of strong absorbers from our two X-shooter samples are consistent with each other to within 0.3σ uncertainties. Using instead $\frac{\partial N}{\partial z}$ from the higher-spectral-resolution quasar data parametrised by Mathes et al. (2017) to compute the expected numbers of absorbers from Eq. (4), we would expect 16.2 and 50.9 strong absorbers, resulting in no evidence for any excess with factors of 1.11 ± 0.29 (GRBs) and 1.02 ± 0.18 (quasars), respectively.

There are several possible causes for a discrepancy between the Mg II absorber incidences in high-resolution data and the SDSS. Choosing to use any available high-resolution quasar spectra in the archives may cause a bias. Particularly, any observing programmes aimed at follow-up DLA studies will force dN/dz to become artificially high for strong Mg II absorbers, while no bias is expected for weak absorbers as weak systems are rarely targeted on purpose. Other observing programmes may have targeted quasars specifically selected to not have strong intervening absorbers. To what extent these selections affect the reported incidences in the literature is unclear. Mathes et al. (2017) noted a slight excess of strong Mg II absorbers compared to SDSS, specifically for the strongest ones with $W_r > 3$ Å. They performed K-S tests on similarly sized samples of weak plus strong absorbers ($W_r > 0.3$ Å) drawn from SDSS quasars, and by comparing the equivalent width distribution functions $f(W_r, W^*) = (N^*/W^*)\exp(-W_0/W^*)$ they found similar characteristic equivalent widths, W^*, and concluded that their high-resolution samples were not biased. They did not compare the strong absorbers alone, nor did they investigate discrepancies in incidences. In a similar manner, Evans et al. (2013) compared the equivalent distribution function of strong Mg II absorbers with that of SDSS absorbers studied by Nestor et al. (2005), and by performing K-S tests they concluded that their samples were not inconsistent within a 2σ level to the SDSS. This is surprising as the incidence data points in Fig. 4 are inconsistent with the SDSS.

We speculate that the automated searches for Mg II absorbers in SDSS may miss some of the absorbers even though the search algorithms take into account S/N and detection limits of the absorbers as well as correcting for incompleteness. However, because different publications of incidences based on SDSS quasars largely agree, we do not consider this a valid explanation. In this work, we have compared the incidence to SDSS incidences by Zhu & Ménard (2013), but note that other authors have measured slightly different incidences from various SDSS data releases. For example, Seyffert et al. (2013) reported $dN/dz(z = 0.36-2.28) = 0.293 \pm 0.002$ while the incidence in this redshift interval in the study by Zhu & Ménard (2013) was $dN/dz = 0.306^{+0.001}_{-0.005}$ and Nestor et al. (2005) reported $dN/dz = 0.278 \pm 0.010$. If we had chosen other references for SDSS incidences, the excess in high-resolution data would have been slightly higher. Nevertheless, the variations between incidences derived from various analysis methods and SDSS data releases are small compared to the excess seen for the high-resolution data.

A third plausible cause for discrepancies is the quasar optical colour-selection criteria adopted by SDSS, which is biased against red, dusty quasars (Krogager et al. 2016; Fynbo et al. 2017). Some of these quasars are reddened by dust in intervening DLAs or by dust in additional strong intervening Mg II absorbers (Heintz et al., in prep.). Heintz et al. estimate that about 10% of quasars are missed by SDSS or the Baryonic Oscillations Spectroscopic Survey (BOSS), whereas Ménard et al. (2008) estimate that only 1% are missed by dust in foreground Mg II absorbers with $W_r = 1$ Å but with a percentage that increases to 50% for the strongest absorbers ($W_r = 6$ Å). Raghunathan et al. (2016) find that about 10% of the 266 433 quasars in SDSS DR12 contain strong Mg II absorbers. If a very large fraction of the missed quasars have strong intervening absorbers, the true Mg II absorber incidence towards quasars could be a factor of 2 higher than seen in SDSS, thereby explaining the excess we see in high-resolution data. The factor of 2 higher incidence is an upper limit because quasars may be reddened by their hosts rather than by intervening absorption systems (Krogager et al. 2015, 2016). To determine if there is a significant excess of strong Mg II absorbers towards these red quasars and to measure the effect of the incidences on SDSS quasar selection biases requires the analysis of the incidence and equivalent distribution function of intervening absorbers towards the reddened quasars. This will be the focus of future work.

Some quasars in the XQ-100 survey are selected from SDSS, so any potential selection biases in SDSS would propagate into

this survey, as well as other high-spectral-resolution quasar studies. Radio-selected quasar samples would not propagate this dust bias, but a comparison of Mg II absorber incidences towards radio- and optically selected quasars did not show any difference (Ellison et al. 2004). The search for strong Mg II absorbers towards blazars (Bergeron et al. 2011) included both radio- and optically (SDSS) selected targets, but with 9 optically selected and very bright targets from a sample of 45 objects, any bias carried by SDSS would be small, and could also cause an excess of Mg II towards blazars like those seen in high-resolution quasar studies.

3.4. Comparison at higher redshifts; $z \gtrsim 2.3$

Because the SDSS spectra only cover visible wavelengths, the Mg II samples extend to only $z \approx 2.3$. Expanding the redshift range by observing higher-redshift quasars with near-IR spectra at an intermediate resolution of $R \sim 6000$ with Magellan/FIRE, Matejek & Simcoe (2012) showed that beyond this redshift, the incidence rate is constant within the uncertainties ($\mathrm{d}N/\mathrm{d}z \sim 0.575-0.325$) out to $z = 5.35$. These values are consistent with our computed incidence rates beyond $z \gtrsim 2$. With an expanded sample of 100 quasars at $3.55 < z < 7.08$ observed with Magellan/FIRE, Chen et al. (2016) found evidence for a redshift evolution and a declining incidence from $z = 2$ to $z = 6$, as illustrated by the star symbols in Figs. 3 and 4.

Using Eq. (4), we computed the expected number of strong systems from the parametrisation of Chen et al. (2016) to be 7 ± 1 and 81 ± 74, whereas we found 4 and 45 towards GRBs and quasars, respectively. This gives excess factors of 0.71 ± 0.34 and 0.56 ± 0.93, as reported in Table 1. Even though our sample of GRBs is larger than in previous studies, the redshift path length ($\Delta z = 13.14$ at $z > 2.3$ in Table 1) is significantly smaller than path lengths in other high-resolution quasar studies (Matejek & Simcoe 2012; Chen et al. 2016), and this causes a higher uncertainty of the measured incidences.

3.5. Excess due to lensing?

Vergani et al. (2009) suggest lensing magnification of part of the UVES sample as a possible explanation of the excess, as high-resolution UVES spectra can be obtained only for bright afterglows. Such bright afterglows could have an increased probability of having strong Mg II intervening systems (causing the magnification) along lines of sight. Indeed, their sample includes one remarkable burst, GRB 060418, which has three strong intervening Mg II systems, two of which lie at $z \sim 0.6$ (Ellison et al. 2006). Prochter et al. (2006b) noted that excluding this remarkable GRB does not significantly change the statistics. An examination of the field with imaging and follow-up spectra of galaxies near to the GRB line of sight suggested some effects of gravitational magnification (Pollack et al. 2009). However, adopting a different lensing configuration based on recent VLT/MUSE data of this field (PI: Schulze) with spectroscopic identifications of the host galaxies of the absorbers (Christensen & Schulze, in prep.) we find that any lensing magnification is very unlikely for this burst. To produce a significant gravitational magnification the nearby hosts would have to be ~3 orders of magnitude more massive than those detected.

For another burst, GRB 030429, a similar conclusion was made that strong gravitational lensing did not cause magnification, although an intervening galaxy was found close to the GRB line of sight (Jakobsson et al. 2004). On a case-by-case basis we still have no evidence that GRBs are gravitationally magnified.

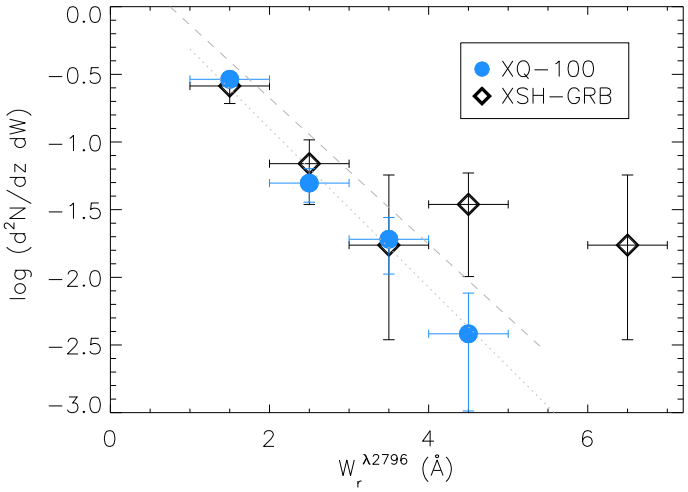

Fig. 5. The equivalent width distribution of W_r^{2796} of the GRB and quasar samples. Vertical error bars were computed using the $\sqrt{N_\mathrm{abs}}$ approximation. The dotted and dashed lines represent best fits for the distribution of quasar absorbers by Mathes et al. (2017) and Chen et al. (2016), respectively.

3.6. The W_r distribution

While we have found that the incidence rates agree between most samples within the uncertainties, the analysis has not considered the distribution of the absorber equivalent widths. We investigate the rest-frame equivalent width distribution by computing the function:

$$f(W) = \frac{\mathrm{d}^2 N}{\mathrm{d}z\mathrm{d}W}. \quad (5)$$

Since our total Mg II sample sizes are not very large, we computed the distribution within the full integrated redshift range. This choice can be justified as Chen et al. (2016) found no significant redshift evolution of the W_r distribution for the strongest absorbers. The results presented in Fig. 5 demonstrate a good overall agreement between the GRB and quasar samples. Although very strong absorbers with $W_\mathrm{r} > 4$ Å appear to be more frequent towards GRBs than quasars, the numbers agree within $\sim 1\sigma$ uncertainty levels. The only outlier is the highest W_r point from the GRB absorbers, which presents a single exceptionally strong Mg II absorber towards GRB 120815A (Krühler et al. 2013). However, the bin only contains a single data point, and within the uncertainties the bin contains $1^{+2.3}_{-0.8}$ absorbers according to Poisson statistics (Gehrels 1986), such that the frequency could be very low as well.

Compared to the W_r distributions from quasar Mg II absorbers in the literature (Chen et al. 2016; Mathes et al. 2017), although marginally consistent within the errors, the absolute values of the GRB sample could suggest a higher frequency of the strongest absorbers. Chen et al. (2016) reported that the very strong absorbers in their quasar sample were mainly found at $z > 1.5$; a trend which we confirm in our GRB and quasar data.

4. Summary

We combined two VLT/X-shooter legacy data sets consisting of quasar and GRB afterglow spectra to explore the incidence rates

of intervening strong Mg II systems with $W_r^{\lambda 2796} > 1$ Å out to $z \sim 5$. With the combination of uniformly selected data, we have covered large redshift path lengths for both samples, although at $z > 2.3$, the quasar sample probes a ten times larger survey path than the GRB sample. Based on number statistics of absorbers we find that:

- There is no discrepancy between the incidence of strong Mg II absorbers at $0.1 < z < 5$ between the two samples. Number statistics show agreements within 1σ uncertainty levels at all redshift bins.
- Our determined incidence of strong Mg II systems towards quasars agrees within 1σ with other intermediate- to high-spectral-resolution ($R \gtrsim 6000$) quasar studies (Evans et al. 2013; Mathes et al. 2017) at redshifts in the range $0.14 < z < 2.6$.
- The decline of the incidence of strong Mg II absorbers at higher redshifts ($2 < z < 6$) towards quasars (Chen et al. 2016) is not seen in our sample. However, we cannot exclude a decline beyond $z \sim 2.5$ due to large uncertainties of the incidences. We do not detect any absorbers beyond $z \sim 4.6$.
- At lower redshifts ($0.14 < z < 2.3$), the incidence of strong Mg II absorbers in the X-shooter data suggests an overdensity of a factor of 1.5 ± 0.4 (GRBs) and 1.4 ± 0.2 (quasars) relative to the large statistical database of strong Mg II absorbers in SDSS quasars (Prochter et al. 2006b; Zhu & Ménard 2013; Raghunathan et al. 2016). The only remaining discrepancy in the incidence of strong Mg II absorbers is therefore between SDSS quasars and higher-spectral-resolution quasar studies. We suggest that this discrepancy can be explained by a selection bias in SDSS against quasars reddened by dust in intervening absorbers.
- Incidences from the low-resolution ($R \lesssim 2000$) GRB afterglow spectra from FORS analysed in this work agree within their 1σ error bars with SDSS quasar data, but also with the X-shooter intermediate-spectral-resolution results due to the large error bars.
- The distribution of absorber equivalent widths with $1 < W_r^{\lambda 2796} < 7$ Å is consistent within 1σ uncertainty levels between the quasar and the GRB afterglow samples. The distributions are also consistent with measurements from high-spectral-resolution studies of quasar absorbers (Chen et al. 2016; Mathes et al. 2017).

The agreement between incidences towards GRB afterglows and quasars demonstrates that both object types probe random lines of sight through the universe. Neither of the objects is more likely than the other to encounter an intervening strong Mg II absorber. The measured incidences and evolution with redshift of both types of line of sight are therefore consistent with the notion that strong Mg II systems can be used as unbiased tracers of the global star formation rate density of the universe out to the highest redshifts (Ménard et al. 2011). Detecting very-high-redshift GRBs with intervening very-high-redshift Mg II absorbers will therefore provide a useful tracer of the star formation density at the earliest epochs in the universe.

Acknowledgements. We acknowledge valuable comments from an anonymous referee. L.C. and R.C. are supported by YDUN grant DFF 4090-00079. S.D.V. is supported by the French National Research Agency (ANR) under contract ANR-16-CE31-0003 BEaPro. S.L. has been supported by FONDECYT grant number 1140838 and partially by PFB-06 CATA. A.d.U.P. and C.T. acknowledge support from Ramón y Cajal fellowships, and with RSR a BBVA Foundation Grant for Researchers and Cultural Creators, and the Spanish Ministry of Economy and Competitiveness through project AYA2014-58381-P. G.B. acknowledges support from the National Science Foundation through grant AST-1615814. Z.C. acknowledges support from the Juan de la Cierva Incorporación fellowship IJCI-2014-21669 and from the Spanish research project AYA 2014-58381-P. P.J. and K.E.H. acknowledge support by a Project Grant (162948–051) from The Icelandic Research Fund. J.J. acknowledges support from NOVA and NWO-FAPESP grant for advanced instrumentation in astronomy. R.S.R. acknowledges support from ASI (Italian Space Agency) through the Contract No. 2015-046-R.0 and from European Union Horizon 2020 Programme under the AHEAD project (grant agreement No. 654215). M.V. gratefully acknowledges financial support from the Danish Council for Independent Research via grant no. DFF 4002-00275.

References

Berg, T. A. M., Ellison, S. L., Sánchez-Ramírez, R., et al. 2016, MNRAS, 463, 3021
Berg, T. A. M., Ellison, S. L., Prochaska, J. X., et al. 2017, MNRAS, 464, L56
Bergeron, J., Boissé, P., & Ménard, B. 2011, A&A, 525, A51
Budzynski, J. M., & Hewett, P. C. 2011, MNRAS, 416, 1871
Chen, S.-F. S., Simcoe, R. A., Torrey, P., et al. 2016, ApJ, submitted [arXiv:1612.02829]
Cucchiara, A., Jones, T., Charlton, J. C., et al. 2009, ApJ, 697, 345
Cucchiara, A., Prochaska, J. X., Zhu, G., et al. 2013, ApJ, 773, 82
de Ugarte Postigo, A., Fynbo, J. P. U., Thöne, C. C., et al. 2012, A&A, 548, A11
de Ugarte Postigo, A., Blazek, M., Janout, P., et al. 2014, in Software and Cyberinfrastructure for Astronomy III, Proc. SPIE, 9152, 91520
Ellison, S. L. 2006, MNRAS, 368, 335
Ellison, S. L., Yan, L., Hook, I. M., et al. 2002, A&A, 383, 91
Ellison, S. L., Churchill, C. W., Rix, S. A., & Pettini, M. 2004, ApJ, 615, 118
Ellison, S. L., Vreeswijk, P., Ledoux, C., et al. 2006, MNRAS, 372, L38
Ellison, S. L., Prochaska, J. X., & Mendel, J. T. 2011, MNRAS, 412, 448
Evans, J. L., Churchill, C. W., Murphy, M. T., Nielsen, N. M., & Klimek, E. S. 2013, ApJ, 768, 3
Frank, S., Bentz, M. C., Stanek, K. Z., et al. 2007, Ap&SS, 312, 325
Freudling, W., Romaniello, M., Bramich, D. M., et al. 2013, A&A, 559, A96
Fynbo, J. P. U., Jakobsson, P., Prochaska, J. X., et al. 2009, ApJS, 185, 526
Fynbo, J. P. U., Krogager, J.-K., Heintz, K. E., et al. 2017, A&A, 606, A13
Gehrels, N. 1986, ApJ, 303, 336
Jakobsson, P., Hjorth, J., Fynbo, J. P. U., et al. 2004, A&A, 427, 785
Krogager, J.-K., Geier, S., Fynbo, J. P. U., et al. 2015, ApJS, 217, 5
Krogager, J.-K., Fynbo, J. P. U., Heintz, K. E., et al. 2016, ApJ, 832, 49
Krühler, T., Ledoux, C., Fynbo, J. P. U., et al. 2013, A&A, 557, A18
Lanzetta, K. M., Turnshek, D. A., & Wolfe, A. M. 1987, ApJ, 322, 739
Lawther, D., Paarup, T., Schmidt, M., et al. 2012, A&A, 546, A67
Lopez, S., D'Odorico, V., Ellison, S. L., et al. 2016, A&A, 594, A91
Matejek, M. S., & Simcoe, R. A. 2012, ApJ, 761, 112
Mathes, N. L., Churchill, C. W., & Murphy, M. T. 2017, ArXiv e-prints [arXiv:1701.05624]
Ménard, B., Nestor, D., Turnshek, D., et al. 2008, MNRAS, 385, 1053
Ménard, B., Wild, V., Nestor, D., et al. 2011, MNRAS, 417, 801
Modigliani, A., Goldoni, P., Royer, F., et al. 2010, in Observatory Operations: Strategies, Processes, and Systems III, Proc. SPIE, 7737, 773728
Mortlock, D. J., Warren, S. J., Venemans, B. P., et al. 2011, Nature, 474, 616
Nestor, D. B., Turnshek, D. A., & Rao, S. M. 2005, ApJ, 628, 637
Pâris, I., Petitjean, P., Ross, N. P., et al. 2017, A&A, 597, A79
Planck Collaboration XIII. 2016, A&A, 594, A13
Pollack, L. K., Chen, H.-W., Prochaska, J. X., & Bloom, J. S. 2009, ApJ, 701, 1605
Pontzen, A., Hewett, P., Carswell, R., & Wild, V. 2007, MNRAS, 381, L99
Porciani, C., Viel, M., & Lilly, S. J. 2007, ApJ, 659, 218
Prochter, G. E., Prochaska, J. X., & Burles, S. M. 2006a, ApJ, 639, 766
Prochter, G. E., Prochaska, J. X., Chen, H.-W., et al. 2006b, ApJ, 648, L93
Raghunathan, S., Clowes, R. G., Campusano, L. E., et al. 2016, MNRAS, 463, 2640
Rapoport, S., Onken, C. A., Wyithe, J. S. B., Schmidt, B. P., & Thygesen, A. O. 2013, ApJ, 766, 23
Salvaterra, R., Della Valle, M., Campana, S., et al. 2009, Nature, 461, 1258
Sánchez-Ramírez, R., Ellison, S. L., Prochaska, J. X., et al. 2016, MNRAS, 456, 4488
Seyffert, E. N., Cooksey, K. L., Simcoe, R. A., et al. 2013, ApJ, 779, 161
Sudilovsky, V., Savaglio, S., Vreeswijk, P., et al. 2007, ApJ, 669, 741
Tanvir, N. R., Fox, D. B., Levan, A. J., et al. 2009, Nature, 461, 1254
Tejos, N., Lopez, S., Prochaska, J. X., Chen, H.-W., & Dessauges-Zavadsky, M. 2007, ApJ, 671, 622
Tejos, N., Lopez, S., Prochaska, J. X., et al. 2009, ApJ, 706, 1309
Vergani, S. D., Petitjean, P., Ledoux, C., et al. 2009, A&A, 503, 771
Vernet, J., Dekker, H., D'Odorico, S., et al. 2011, A&A, 536, A105
Zhu, G., & Ménard, B. 2013, ApJ, 770, 130

Appendix A: Additional table

Table A.1. Intervening absorbers in the QSO sample.

QSO name	z_{QSO}	z_{abs}	$W_r^{\lambda 2796}$ [Å]
J0003–2603	4.12	3.3899	1.318 ± 0.012
J0006–6208	4.44	1.9580	1.845 ± 0.021
		3.7762	1.100 ± 0.029
J0034+1639	4.29	1.7997	1.556 ± 0.016
		2.8524	1.270 ± 0.064
J0042–1020	3.86	2.7545	1.929 ± 0.018
		3.6286	1.158 ± 0.027
J0056–2808	3.63	1.3411	1.221 ± 0.020
J0100–2708	3.55	2.1484	1.366 ± 0.019
J0113–2803	4.31	1.3898	1.506 ± 0.017
		3.0160	4.000 ± 0.066
J0117+1552	4.24	2.5227	3.041 ± 0.029
J0124+0044	3.84	2.2609	1.603 ± 0.015
J0134+0400	4.18	1.6656	1.637 ± 0.010
		3.7725	2.287 ± 0.014
J0137–4224	3.97	3.1010	1.013 ± 0.096
J0153–0011	4.19	1.9080	1.126 ± 0.040
J0211+1107	3.97	1.4689	1.780 ± 0.022
		2.5250	1.318 ± 0.036
		3.1415	1.533 ± 0.031
		3.5033	1.685 ± 0.044
J0214–0518	3.98	1.3071	1.075 ± 0.013
		1.5279	2.901 ± 0.018
J0234–1806	4.30	3.6934	2.182 ± 0.053
		4.2280	1.877 ± 0.047
J0244–0134	4.05	2.1011	1.688 ± 0.016
J0247–0555	4.23	1.7099	1.176 ± 0.019
J0255+0048	4.00	3.2551	2.576 ± 0.032
		3.4502	0.972 ± 0.027
J0307–4945	4.72	2.6288	1.047 ± 0.036
		3.5909	1.379 ± 0.015
		4.2110	2.038 ± 0.020
		4.4658	1.665 ± 0.019
J0311–1722	4.03	1.9408	1.321 ± 0.014
J0415–4357	4.07	3.8076	2.102 ± 0.024
J0424–2209	4.33	4.1418	0.983 ± 0.023
J0523–3345	4.39	1.5705	1.056 ± 0.010
J0529–3526	4.42	2.1907	1.588 ± 0.041
J0747+2739	4.13	2.6100	2.435 ± 0.184
		3.4221	1.511 ± 0.025
J0818+0958	3.66	2.8270	1.124 ± 0.033
		3.3061	1.532 ± 0.028
J0833+0959	3.72	1.2911	2.224 ± 0.014
J0835+0650	4.01	1.5096	1.727 ± 0.018
		3.1894	1.181 ± 0.036
J0839+0318	4.23	2.1340	1.375 ± 0.065
J0920+0725	3.65	1.5790	1.206 ± 0.010
		2.1437	1.266 ± 0.012
		2.2368	1.331 ± 0.012
J0935+0022	3.75	1.2827	2.787 ± 0.027
J0937+0828	3.70	2.1440	2.260 ± 0.021
J0955–0130	4.42	2.6235	1.859 ± 0.123
J0959+1312	4.09	1.8727	2.850 ± 0.012
J1020+0922	3.64	1.8055	1.110 ± 0.023
J1032+0927	3.98	2.2617	0.997 ± 0.017
J1034+1102	4.27	1.6004	1.992 ± 0.012
		2.1167	2.377 ± 0.013
J1042+1957	3.63	2.1424	1.052 ± 0.018
J1054+0215	3.97	1.4944	1.616 ± 0.025
J1057+1910	4.13	1.9853	1.285 ± 0.044
		3.3735	2.361 ± 0.095
J1058+1245	4.34	3.4305	1.501 ± 0.038
		2.1097	3.079 ± 0.019
		2.1826	1.569 ± 0.025
J1103+1004	3.61	1.7543	1.148 ± 0.015
J1108+1209	3.68	1.8693	2.376 ± 0.019
		3.5450	1.761 ± 0.025
J1110+0244	4.14	2.1199	3.021 ± 0.015
J1111–0804	3.92	1.9769	1.798 ± 0.015
J1201+1206	3.52	1.9973	1.541 ± 0.007
J1202–0054	3.59	2.7696	0.986 ± 0.036
J1249–0159	3.63	3.1020	1.786 ± 0.022
J1304+0239	3.65	1.8075	1.330 ± 0.013
		3.2108	4.699 ± 0.023
J1312+0841	3.73	1.9183	1.155 ± 0.013
		2.6594	1.138 ± 0.054
J1320–0523	3.72	1.4038	1.969 ± 0.013
		1.5277	1.488 ± 0.012
J1323+1405	4.05	1.4974	1.048 ± 0.020
		1.9824	1.634 ± 0.041
J1330–2522	3.95	3.0810	1.426 ± 0.019
J1331+1015	3.85	1.5793	1.122 ± 0.016
J1352+1303	3.71	3.0075	2.106 ± 0.024
J1416+1811	3.59	2.1150	1.145 ± 0.018
		2.2277	2.449 ± 0.019
J1421+0643	3.69	1.4580	1.539 ± 0.014
		2.6158	1.178 ± 0.073
J1442+0920	3.53	1.1233	1.048 ± 0.013
J1524+2123	3.60	2.5449	0.997 ± 0.133
J1542+0955	3.99	3.2818	1.091 ± 0.056
J1552+1005	3.72	3.6665	1.772 ± 0.037
J1621–0042	3.71	1.1341	3.167 ± 0.016
		3.1050	1.504 ± 0.020
J1633+1411	4.36	2.2345	1.007 ± 0.015
J1723+2243	4.53	3.6958	3.762 ± 0.018
J2215–1611	3.99	2.3910	1.284 ± 0.018
J2216–6714	4.48	2.0615	1.455 ± 0.011
J2239–0522	4.55	3.0310	1.537 ± 0.020
J2251–1227	4.16	2.8826	1.796 ± 0.039
J2344+0342	4.25	2.5541	1.156 ± 0.040
		3.2201	1.458 ± 0.018
J2349–3712	4.22	2.8305	1.477 ± 0.064

Notes. Quasar and strong Mg II system redshifts are listed as z_{QSO} and z_{abs}.